CHEMISTRY
A EUROPEAN JOURNAL

DOI: 10.1002/chem.201000758

Durability Improvement of a Pt Catalyst with the Use of a Graphitic Carbon Support

Bao Yu Xia,[a] Jian Nong Wang,*[b] Shang Jun Teng,[a] and Xiao Xia Wang[c]

Proton-exchange membrane fuel cells (PEMFC) with a low operation temperature, high power density, prompt startup and no pollution have attracted much attention as the new energy source for automobiles, portable electronic devices, and distributed home power sources.[1] However, the commercialization of PEMFC is hindered by several deficiencies such as lifetime, reliability, and cost.[2] Thus, there is a rapid growing interest in the investigation of the performance degradations of PEMFC and its component materials.[3] The durability of carbon-supported Pt catalysts is of significance not only for lengthening the operation life, but also for enhancing the reliability and reducing the total lifetime cost of PEMFC.[4]

To improve the catalyst durability, the traditional catalyst of Pt has been alloyed with a second and/or even a third metal.[5] Nevertheless, common problems exist for all alloyed catalysts. Notably, the activities of these catalysts are usually lower than the unalloyed ones. Furthermore, the nonprecious metals in alloys such as PtNi,[6] PtCo,[7] and PtCu[8] suffer from dissolution in acid solutions, and the dissolution results in further decreases of the catalytic activity and cell performance.[9] In parallel, efforts have also been made to search for new support materials to replace the currently widely used carbon black (CB; Vulcan XC-72).[9,10] Some new carbon materials such as carbon nanotubes (CNTs),[11] nanocoils,[12] and nanoporous carbons[13] have been examined as alternative catalyst supports. Particularly, CNTs as the catalyst support have been widely reported. However, most of the CNTs synthesized by arc discharge, laser evaporation, and chemical vapor deposition exhibit a low surface area and a low yield with a high proportion of impurities, and the subsequent purification is complex.[14] Although CNTs have a unique structure and high crystallinity, they tend to aggregate into bundles owing to the substantial van der Waals attractions. These bundles are usually entangled to form larger aggregates, leading to difficult dispersion and limiting the practical application of CNTs.[15] Therefore, the advantage of the use of these new nanocarbons is still not clear and achieving a high durability without scarifying the actual activity is still a huge technical challenge.

In this paper, we report a new approach for developing a catalyst with both high activity and durability. This is based on the use of carbon nanocages (CNCs) with a graphitic structure as the catalyst support.[16] Both the new Pt catalyst supported on CNCs (Pt/CNC) and the conventional ones on CB (Pt/CB) have been studied. The thermal stability was examined after the catalyst had been exposed in air at a temperature of 120 °C for up to 1000 h, and the electrochemical durability was tested under acidic conditions similar to those in low-temperature fuel cells.[17] From these experiments, a clear understanding of the degradation of carbon-supported catalysts over time under a range of conditions of relevance to PEMFC operation can be gained. This understanding will be useful for the future design of catalysts with a higher activity and stability and will also assist in the improvement of the fuel cell performance.

The present support material is a graphitic carbon consisting of CNCs. The synthetic process and characteristics of the CNCs have been reported in our previous publications.[16] The phase constitution and structure of CNCs and CB were analyzed by using XRD as shown in Figure 1a. The peaks at $2\theta = 26.2$ and 44.4° can be attributed to the diffractions of the (002) and (101) planes of the hexagonal structure of graphite, respectively. The peaks of CNCs are sharper and narrower than those for CB, indicating a much better graph-

[a] B. Y. Xia, S. J. Teng
Shanghai Key Laboratory for Laser Processing and Materials Modification, School of Materials Science and Engineering
Shanghai Jiao Tong University, 800 Dong Chuan Road
Shanghai 200240 (P.R. China)

[b] Prof. J. N. Wang
Key Laboratory of Safety Science of Pressurized System (Ministry of Education), School of Mechanical and Power Engineering
East China University of Science and Technology
130 Meilong Road, Shanghai 200237 (P.R. China)
Fax: (+86) 21-6598 5385
E-mail: jnwang@sjtu.edu.cn

[c] Dr. X. X. Wang
Shanghai Key laboratory for Metallic Functional Materials
School of Materials Science and Engineering
Tongji University, 1239 Siping Road, Shanghai 200092 (P.R. China)

Supporting information for this article is available on the WWW under http://dx.doi.org/10.1002/chem.201000758.

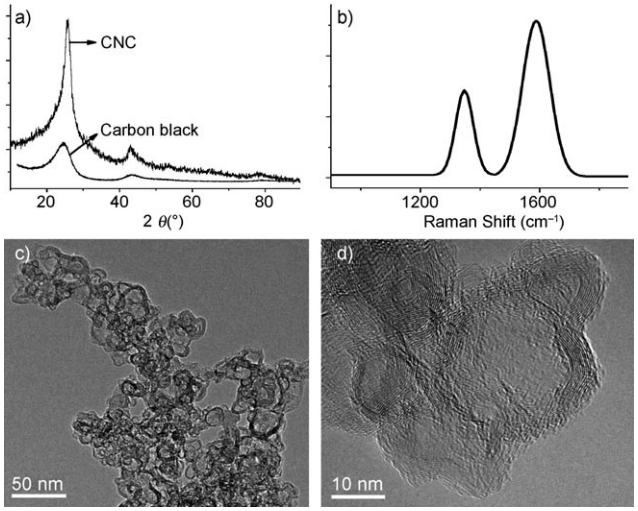

Figure 1. a) XRD patterns, b) Raman spectroscopy, and c) and d) HRTEM images of CNCs.

itic degree than CB. The present CNCs were further characterized by Raman spectroscopy (Figure 1b). The spectrum illustrates two main peaks at 1587 (G band) and 1345 cm^{-1} (D band). The G band corresponds to the E_{2g} vibration of graphitic carbon with a sp^2 electronic configuration. On the other hand, the D band is associated to the A_{1g} mode of diamond-like carbon with a sp^3 configuration. The graphitic degree of a carbon material is evaluated by using the relative intensity ratio of the G band (I_G) and D band (I_D). The I_G/I_D ratio for CNCs has been calculated to be 1.83 (>1), which indicates that CNCs have a very good crystalline structure. Furthermore, the microstructure of CNCs is observed from HRTEM images (Figure 1c and d). The CNCs have a hollow interior and a graphitic shell, and their sizes are generally in the range of 20 to 50 nm. The nitrogen adsorption/desorption isotherms of the CNCs and CB are shown in the Supporting Information. The BET specific surface area of CNCs is measured to be 420 $m^2 g^{-1}$ and results mainly from mesopores, and that of CB is measured to be 200 $m^2 g^{-1}$ and results mainly from micropores (Figure S1 in the Supporting Information).

Pt nanoparticles were deposited on CNCs and CB. The constituent crystalline phases and structures of the Pt/CNC and Pt/CB catalysts before and after thermal exposure were examined by means of XRD analysis and the results are shown in Figure 2. The peaks at about 39.7, 46.3, and 67.4° can be assigned to the (111), (200), and (220) planes of Pt, respectively. After thermal exposure in air, the intensities of the Pt peaks become stronger with the increase of thermal exposure time. The average Pt particle size was calculated based on the Pt (220) peak from Scherrer's equation, $d=0.9\lambda/B\cos\theta$ in which d is the average particle size (nm), λ is the wavelength of X-ray radiation, and B is the width (in radius) of the diffraction peak at the half height. The average crystalline sizes of the Pt particles are presented in Table 1. The Pt particle sizes of both Pt/CNC and Pt/CB catalysts increased rapidly in the first 300 h, but remained almost unchanged after 300 h.

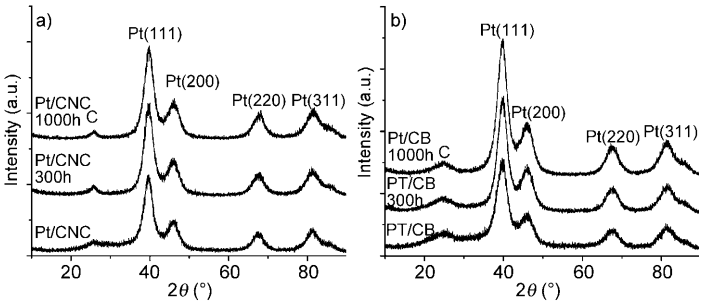

Figure 2. XRD patterns of a) Pt/CNC and b) Pt/CB after different amounts of thermal exposure.

Typical images of the original Pt/CNC sample are shown in Figure 3a and b. As can be seen, the Pt particles are

Table 1. Pt particle sizes and electrochemical surface areas (ESA) of different catalysts calculated from XRD patterns and CV profiles, respectively.

Sample	Pt/CNC			Pt/CB		
thermal exposure time [hours]	0	300	1000	0	300	1000
size [nm]	2.8	3.6	4.0	3	3.8	4.4
ESA [$m^2 g^{-1}$]	82	62	60	69	39	35

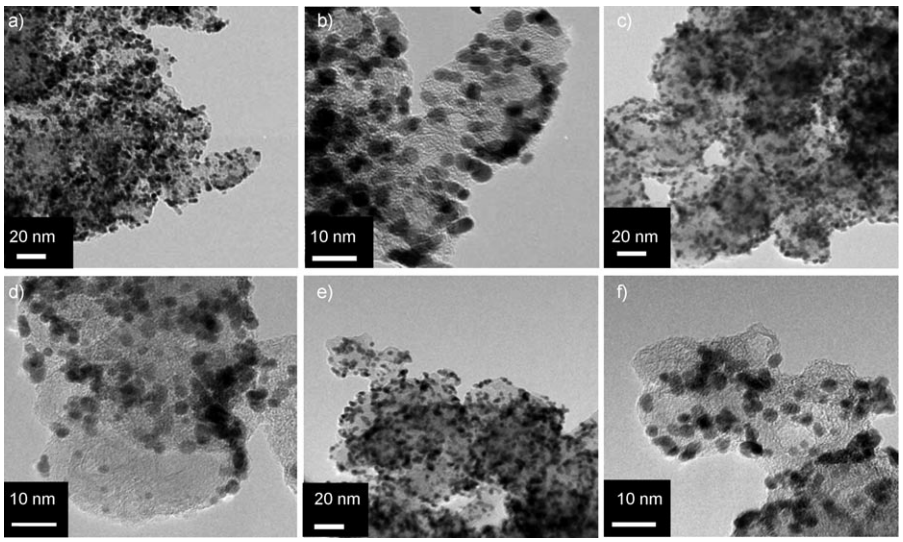

Figure 3. TEM images of Pt/CNC after different amounts of thermal exposure: a) and b) Original samples, c) and d) after 300 h, e) and f) after 1000 h.

highly dispersed on the CNC surfaces. By counting hundreds of Pt nanoparticles on representative TEM images, the average size for Pt particles is estimated to be 3.0 nm, which is in close agreement with that estimated by Scherrer's equation (2.8 nm). The TEM images of the Pt/CNC sample after thermal exposure for a different number of hours are shown in Figure 3c and d (300 h) and Figure 3e and f (1000 h). It was found that Pt nanoparticles display a visible conglomeration during the first 300 h and the conglomeration becomes little noticeable in the subsequent exposure. The average sizes of the Pt particles on CNCs are 3.8 and 4.0 nm for the 300 and 1000 hour samples, respectively. Figure 4 displays the TEM images of Pt/CB. From Figure 4a and b, the Pt nanoparticle size of the original sample was approximately 3.3 nm, and after 1000 h of thermal exposure the size increased to approximately 5.0 nm (Figure 4c and d).

Figure 5a displays the cyclic voltammogram (CV) results of the Pt/CNC catalyst after different amounts of thermal exposure at 120°C. In general, the intensity of adsorption/desorption peaks shows a downtrend with the exposure time. Furthermore, the peaks of both hydrogen and oxygen redox at approximately 0.2 and 0.7 V decrease quickly in the first 300 h, but remain stable from 300 to 1000 h.

In Figure 5, the current density of 40 mA cm^{-2} at approximately −0.1 V corresponds to the weak hydrogen desorption and that of 42 mA cm^{-2} at approximately −0.01 V corresponds to the strong hydrogen desorption for the original sample. These two peaks are normally attributed to Pt (111) and (100) crystal planes.[18] After 300 h of thermal exposure in air, the weak H_2 desorption peak drops slightly to approximately 36 mA cm^{-2} and the strong H_2 desorption peak stabilizes at approximately 33 mA cm^{-2}. At the same time, the peak at approximately −0.03 V, which is usually related to Pt(110), is clearly observed (Figure 5a).[18] The current density of this peak drops down from approximately 43 to 34 mA cm^{-2}. When the thermal exposure time was extended to 1000 h, the intensity change of these hydrogen desorption peaks was very little.

The ESA ($m^2 g^{-1}$) is generally believed to be one of the important parameters for characterizing fuel cell performance. The ESA is estimated from [Eq. (1)] in which Q is the charge for hydrogen desorption (mC cm^{-2}), m is the quantity of Pt used (=0.4 mg cm^{-2} in the present study), and β the

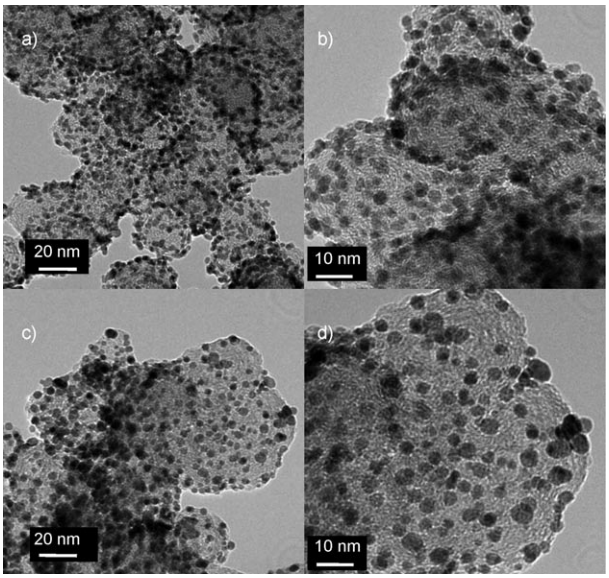

Figure 4. TEM images of Pt/CB after different amounts of thermal exposure: a) and b) Original samples, c) and d) after 1000 h.

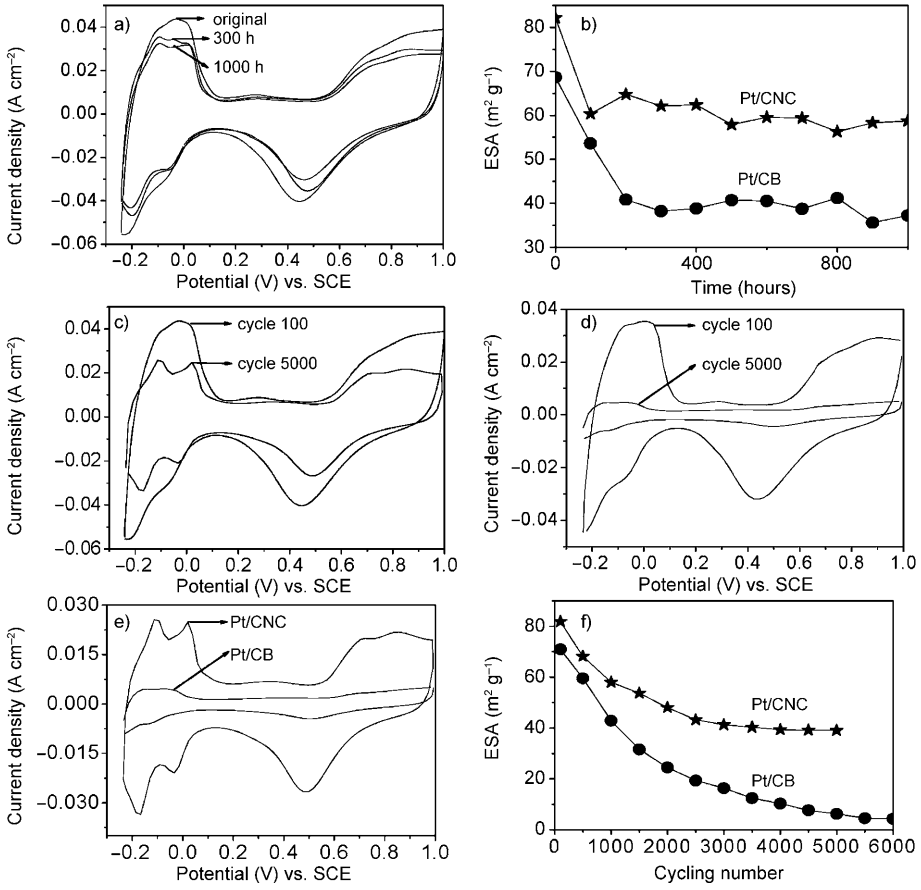

Figure 5. a) CVs of Pt/CNC, b) ESA variation with thermal exposure time, c) CVs of accelerated durability tests of Pt/CNC, d) CVs of accelerated durability tests of Pt/CB, e) CVs profiles of Pt/CNC and Pt/CB after 5000 cycles selected from c) and d), f) ESA variation with cycling number.

charge required to oxidize a monolayer of H_2 on bright Pt ($=0.21$ mC cm^{-2}).[19]

$$ESA = Q/(m\beta) \quad (1)$$

The Q value for each catalyst can be calculated from its cyclic voltammogram. In doing this, the contribution of the charge from the electric double layer to the overall amount of charge exchanged during the electroadsorption/desorption of H_2 on the Pt sites was deducted. Such calculated values of effective α for different catalysts are plotted in Figure 5b.

The ESA of the original Pt/CNC sample is as high as 82 m^{2}g^{-1}. Furthermore, the ESA decreases to 65 m^{2}g^{-1} within the first 300 h, and shows only a small fluctuation after 300 h (from 65 to 60 m^{2}g^{-1}). However, in the case of the Pt/CB catalyst, the ESA decreases rapidly from 69 to 39 m^{2}g^{-1} in the first 300 h and from 39 to 35 m^{2}g^{-1} as the exposure is extended.

The chemical composition on the surfaces of Pt/CNC and Pt/CB catalysts before and after thermal exposure were analyzed by XPS (Figure 6). The elemental composition of the catalysts can be calculated and they are presented in Table 2. The regional scan for Pt element provides the valence states of the Pt existing in the catalysts. As shown in Figure 6b, the Pt signal consists of three pairs of doublets. The most intense doublet (71.2 and 74.7 eV) is due to metallic Pt^0. The second set of doublets (71.8 and 75.4 eV) could be assigned to the Pt^{II} chemical state as PtO. The third doublet of Pt is the weakest in intensity at even higher binding energies (72.6 and 76.6 eV), which are most likely caused by a small amount of Pt^{IV}. The percentage of Pt^0 can be represented by the relative peak area of the doublet peaks at 71.2 and 74.7 eV. The results are included in Table 2. As shown, the content of Pt^0 decreased for both of the samples after thermal exposure, and the decrease for Pt^0 in Pt/CB was much more remarkable. The narrow-scan spectra for C and O elements are shown in Figures S2 and S3 in the Supporting Information. As can be seen, there is a little change in the contents of Pt and C on Pt/CNC and only a slight increase in the content of O. However, the contents of Pt and O on Pt/CB increase clearly from 48.35 to 55.57% and from 6.76 to 10.78%, respectively. During this time, the C content decreases from 44.39 to 33.65%. Moreover, the O/C atomic ratio increases from 0.1 for both original samples to 0.15 for Pt/CNC and 0.2 for Pt/CB after 1000 h of thermal exposure (Table 2).

Table 2. The mass percentages obtained from XPS analysis of Pt, C, and O elements, the O/C atomic ratio, and Pt4f relative peak areas in the catalysts.

Sample	Pt/CNC			Pt/CB	
thermal exposure time [hours]	0	300	1000	0	1000
Pt	51.07	50.09	51.47	48.35	55.57
C	42.52	42.2	40.56	44.39	33.65
O	6.41	7.71	7.97	6.76	10.78
O/C atomic ratio	0.1	0.14	0.15	0.1	0.2
Pt^0 relative peak area [%]	46.4	35.8	35.4	42.8	26.5

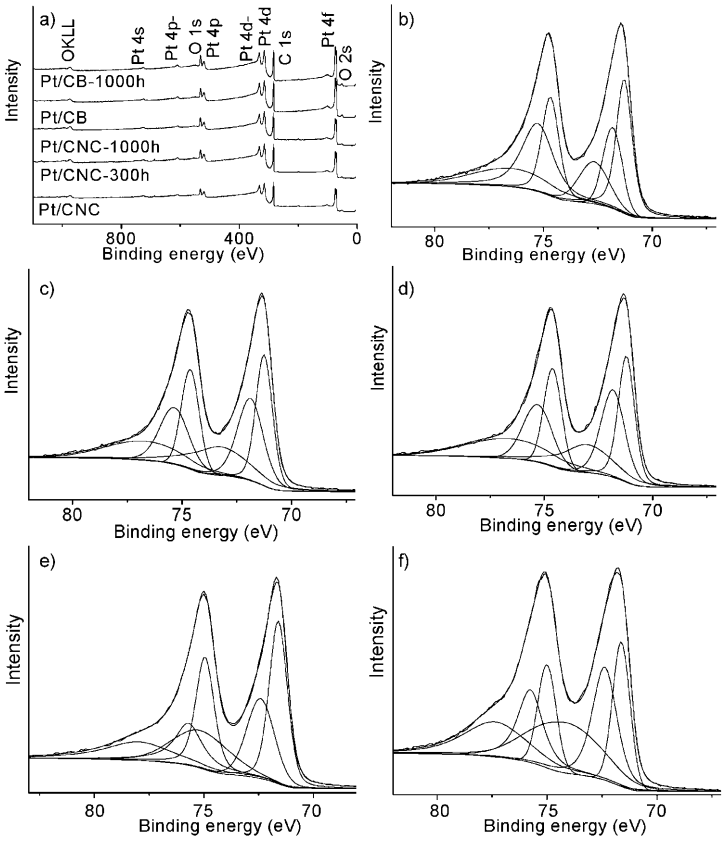

Figure 6. a) Wide-scan XPS spectra of Pt/CNC and Pt/CB with different thermal exposure times. The corresponding Pt4f core level XPS spectra of Pt/CNC: b) Original Pt/CNC; c) Pt/CNC, 300 h; d) Pt/CNC, 1000 h; e) original Pt/CB; f) Pt/CB, 1000 h.

To investigate the electrochemical durability of the catalyst involved, accelerated durability testing (ADT) was conducted in a renewable H_2SO_4 solution (0.5 M) with the catalyst layer exposed to the electrolyte solution to mimic the environment of the electrode membrane interface in PEMFC. Under this specific condition, the deterioration of a catalyst was accelerated. As shown in Figure 5c, after 5000 cycles (about 40 h) the current density dropped from 38 to 25 mA cm^{-2} and from 42 to 25 mA cm^{-2} for the peaks at -0.11 and 0.01 V, respectively, with a scan rate of 100 mV s^{-1}. Compared with Pt/CB (Figure 5d), the current density dropped from 33.7 to 4 mA cm^{-2} and from 34 to 4 mA cm^{-2} for the peaks at -0.02 and -0.007 V, respectively. The loss of the electrochemical surface area (ESA) of the Pt catalyst with the cycling number is plotted in Figure 5f. After 5000 cycles, the ESA decreased from 82 to 41 m^{2}g^{-1} for Pt/CNC (by 50%), and from 71 to 6.3 m^{2}g^{-1} for Pt/CB (by 91.1%). Therefore, the degradation rate of Pt/CB is much faster than that of Pt/CNC. Furthermore, most of the ESA loss for the case of Pt/CNC occurs within 2500 cycles and then the degradation becomes very small. On the contrary, the ESA loss of the Pt/CB catalyst continues to decline during the whole ADT process. These data unambigu-

ously demonstrate that the Pt/CNC catalyst is much more stable than the Pt/CB catalyst.

The electrochemical activity and durability of Pt catalysts have been studied from the aspects of the Pt particles and carbon supports.[20] For the present catalysts, the Pt particle size changed only from 2.8 to 3.6 nm for Pt/CNC and from 3 to 3.8 nm for Pt/CB mainly during the first 300 h of thermal exposure (Figures 2–4). So Pt nanoparticles exist in a relatively stable state even after undergoing long thermal exposure (1000 h). Thus, the big differences in ESA and thermal stability between the two catalysts of Pt/CNC and Pt/CB may be caused by the differences in carbon support and its degradation.

The oxidation of a carbon support usually occurs at the surface. The surface chemistries of the original and thermally exposed Pt/CNC and Pt/CB catalysts were characterized with XPS. Both survey and high-resolution XPS spectra were collected (Figure 6 and Figures S2 and S3 in the Supporting Information). The O1s signal intensity was enhanced for the Pt catalysts, which implies an increase of the oxygen content after a long time of thermal expose, especially for Pt/CB. Pt/CNC shows no obvious change in the high-resolution C1s XPS spectrum, but Pt/CB exhibits weaker signals at approximately 284.7 eV, which is commonly attributed to the fact that carbon–carbon double bonds are broken down. The atomic ratio of O/C, which can be obtained by integrating the area under the high-resolution XPS O1s and C1s spectra signals, is used to monitor the oxygen content and the oxidation degree of a carbon support.[11b,21] The values of O/C for the original, 300 h, and 1000 h Pt/CNC samples are 0.1, 0.14, and 0.15, respectively. The values for the original and 1000 h Pt/CB samples are 0.1 and 0.2, respectively. It is clear that the increase in the atomic ratio O/C for Pt/CB is two times that for Pt/CNC, which indicates that the oxidation degree of CB is much higher than CNCs.

The consequence of carbon oxidation is the weaker interaction between Pt and the carbon support. The exact nature of the interaction is still a topic of considerable discussion.[10b,22] However, in comparison with amorphous carbon, the graphitic structure of a graphitic carbon enhances the strength of the delocalized π sites.[9] These sites act as anchoring centers for Pt nanoparticles, thus strengthening the interaction between the Pt particles and the carbon support.[23] Furthermore, because of the presence of oxygen, surface oxides might weaken the Pt–carbon interaction and lead to a lower resistance to the surface migration of the Pt particles.[8,24] The thermal exposure testing indicates that the effect of carbon support on the degradation is predominant and a graphitic carbon is favorable, and thus efforts should be made to ameliorate the catalyst stability.

The other important observation is that the Pt states have undergone some changes during the long thermal exposure. The percentage of Pt states are calculated from the relative areas of the peaks in Figure 6. The peak positions and all related data are listed in Table 2 and Figure S1 in the Supporting Information. It was found that the percentage of Pt^0 decreased and the contents of Pt^{II} and Pt^{IV} increased with prolonged thermal exposure. The Pt nanoparticles with a small size can be easily oxidized to form a thin oxide shell. This oxidation shell cannot adsorb hydrogen and thus results in electrochemical passivity.[25] As a result, the ESA decreases with thermal exposure for both catalysts studied.

In general, the electrochemical stability of a catalyst could be examined in an electrolyte of a strong aqueous acid solution.[26] It is clearly indicated that the Pt/CNC catalyst showed a higher electrochemical activity and durability by using the Pt/CB catalyst as the baseline (Figure 5). The main phenomenon in acid environments is material dissolution.[27] However, carbon corrosion has a more important effect than Pt degradation (electrode cycling) on the stability of the catalyst.[3b,28] In the CV profile (Figure 5c and d), the decrease in the double-layer capacitance by about 75% for Pt/CB was recorded after the Pt degradation test, but no significant change for Pt/CNC was observed. This effect is clearly related to the corrosion of the amorphous carbon support.[29] Thus, the advantage of a graphitic carbon support is shown again.

In summary, two different Pt catalysts with different support materials (conventional CB and newly developed CNCs) were investigated for thermal stability in air at 120 °C and for electrochemical durability in an acid aqueous solution. Although the Pt size has an effect on electrochemical activity and stability, the effect of carbon oxidation on the thermal degradation is predominant. After long thermal exposure, the electrochemical activity of Pt/CNC decreases by 25%, but that of Pt/CB by 50%. This result indicates that Pt/CNC has a higher thermal stability. In accelerated electrochemical tests, the electrochemical surface area of Pt/CNC decreased by 50%, but that of Pt/CB decreased by 91% under otherwise identical acid conditions after 5000 cycles. All of these observed differences may be attributed to the different carbon materials used to support the Pt particles. This work suggests that by using graphitic carbon materials the thermal stability and electrochemical durability of Pt catalysts can be improved over the conventional amorphous carbon, and thus can be expected to enhance fuel cell performance.

Experimental Section

Preparation of the Pt/Carbon catalysts: The preparation of CNCs has been reported in our previous publications. The typical procedure for preparing the Pt catalyst is the carbon powder was ultrasonicated in ethylene glycol (EG) to form a dispersed solution. Then, a predetermined amount of a Pt precursor, $H_2PtCl_6{\cdot}6H_2O$ dissolved in EG was slowly added. The mixed solution was heated at a desired temperature of around 140 °C for 3 h under continuous magnetic stirring. After cooling to room temperature, the catalyst was then filtered, and washed with excess deionized water until chloride ions were not detected by $AgNO_3$ solution. The Pt loading on the carbon support was controlled to be 50 wt%. Such catalysts prepared by using CNCs and Vulcan XC-72 CB as supports are denoted as Pt/CNC and Pt/CB, respectively.

Measurement of thermal stability and electrochemical durability: The obtained Pt catalyst was placed in an oven with dry air at 120 °C for up to 1000 h to simulate the reaction condition in the low-temperature fuel cell

system. At an interval of 100 h, a small amount of the sample (Pt/CNC, Pt/CB) was taken out of the oven for electrochemical analysis by using a cyclic voltammetry technique. That is, the analysis was performed in a three-electrode cell by using an EG&G potentiostat (model 366A) at ambient temperature. The working electrode was a glassy carbon cylinder with a diameter of 3 mm. The top of the cylinder was coated by the mixture of the Pt catalyst with 5% Nafion isopropanol solution and the Pt loading was controlled at 0.4 mg cm^{-2}. A saturated calomel electrode (SCE) and a large-area Pt plate were used as the reference electrode and counter electrode, respectively, and H_2SO_4 (0.5 M) was used as the electrolyte. The CV profiles were recorded at a scan rate of 100 mV s^{-1} from the potential of −0.241 to 1.0 V versus SCE. For the electrochemical durability test, the recording was made up to 5000 cycles in a renewable aqueous solution of H_2SO_4 (0.5 M) at a scan rate of 100 mV s^{-1}. For comparison, the Pt/CNC and Pt/CB catalysts were studied under identical conditions.

Characterization: The XRD pattern was recorded by using a Bruker diffractometer with $Cu_{K\alpha}$ radiation (Bruker D8 Advanced, 40 kV and 40 mA) to study the phase constitution and crystallographic structure of the sample. Raman spectroscopy was carried out to examine the perfection of CNCs by using Horiba Jobin Yvon HR 800 UV with a 514.5 nm excitation wavelength laser. The morphology of a sample was studied by HR-TEM (JEOL-2010F). EDS was carried out to analyze the chemical composition of the selected area. The surface of the catalysts was analyzed with XPS (Kratos Axis Ultra DLD X-ray photoelectron spectroscopy). This system uses a focused monochromated $Al_{K\alpha}$ (15 kV) X-ray source for excitation and a spherical section analyzer. The pressure of the analyzer chamber was maintained at 10^{-9} Pa during the measurement. The survey scans were collected by using a pass energy of 160 eV. High-resolution spectra were obtained with the analyzer pass energy set as 40 eV. N_2 adsorption experiments by using a BELSORP instrument (BEL, Japan) were conducted to investigate the porosity of hollow CNCs. All samples were outgassed at 200 °C in nitrogen flow for 4 h prior to the measurement. Nitrogen adsorption data were recorded at liquid nitrogen temperature (77 K).

Acknowledgements

J.N.W. is thankful to the research fund (project number 50871067) from The National Natural Science Foundation of China and the fund for the national 863 project of 2007AA05Z128 from The Ministry of Science and Technology of China.

Keywords: catalysis · durability · fuel cells · graphitic carbon · nanoparticles

[1] R. Service, *Science* **2002**, *296*, 1222–1224.
[2] a) H. A. Gasteiger, N. M. Markovic, *Science* **2009**, *324*, 48–49; b) J. Wu, X. Z. Yuan, J. J. Martin, H. Wang, J. Zhang, J. Shen, S. Wu, W. Merida, *J. Power Sources* **2008**, *184*, 104–119.
[3] a) M. Tada, S. Murata, T. Asakoka, K. Hiroshima, K. Okumura, H. Tanida, T. Uruga, H. Nakanishi, S. Matsumoto, Y. Inada, M. Nomura, Y. Iwasawa, *Angew. Chem.* **2007**, *119*, 4388–4393; *Angew. Chem. Int. Ed.* **2007**, *46*, 4310–4315; b) F. A. de Bruijn, V. A. T. Dam, G. J. M. Janssen, *Fuel Cells* **2008**, *8*, 3–22; c) S. Uhm, H. J. Lee, Y. Kwon, J. Lee, *Angew. Chem.* **2008**, *120*, 10317–10320; *Angew. Chem. Int. Ed.* **2008**, *47*, 10163–10166; d) S. D. Knights, K. M. Colbow, J. St-Pierre, D. P. Wilkinson, *J. Power Sources* **2004**, *127*, 127–134; e) S. Y. Huang, P. Ganesan, S. Park, B. N. Popov, *J. Am. Chem. Soc.* **2009**, *131*, 13898–13899; f) S. Kundu, T. C. Nagaiah, W. Xia, Y. Wang, S. V. Dommele, J. H. Bitter, M. Santa, G. Grundmeier, M. Bron, W. Schuhmann, M. Muhler, *J. Phys. Chem. C* **2009**, *113*, 14302–14310.
[4] E. Antolini, J. R. C. Salgado, E. R. Gonzalez, *J. Power Sources* **2006**, *160*, 957–968.
[5] E. Antolini, *Mater. Chem. Phys.* **2003**, *78*, 563–673.
[6] H. R. C. Mercado, H. Kim, B. N. Popov, *Electrochem. Commun.* **2004**, *6*, 795–799.
[7] S. C. Zignania, E. Antolin, E. R. Gonzaleza, *J. Power Sources* **2008**, *182*, 83–90.
[8] G. Gupta, D. A. Slanac, P. Kumar, J. D. W. Camacho, X. Wang, S. Swinnea, K. L. More, S. Dai, K. J. Stevenson, K. P. Johnston, *Chem. Mater.* **2009**, *21*, 4515–4526.
[9] Y. Shao, G. Yin, Y. Gao, *J. Power Sources* **2007**, *171*, 558–566.
[10] a) Y. Shao, J. Liu, Y. Wang, Y. Lin, *J. Mater. Chem.* **2009**, *19*, 46–59; b) E. Antolini, *Appl. Catal. B* **2009**, *88*, 1–24.
[11] a) X. Wang, W. Li, Z. Chen, M. Waje, Y, Yan, *J. Power Sources* **2006**, *158*, 154–159; b) Y. Shao, G. Yin, Y. Gao, P. Shi, *J. Electrochem. Soc.* **2006**, *153*, A1093–A1097.
[12] a) T. Hyeon, S. Han, Y. Sung, K. W. Park, Y. W. Kim, *Angew. Chem.* **2003**, *115*, 4488–4492; *Angew. Chem. Int. Ed.* **2003**, *42*, 4352–4356; b) J. Du, C. Song, J. Zhao, Z. Zhu, *Appl. Surf. Sci.* **2008**, *255*, 2989–2993.
[13] a) S. K. Natarajan, J. Hamelin, *J. Electrochem. Soc.* **2009**, *156*, B210–215; b) R. Kou, Y. Shao, D. Wang, M. H. Engelhard, J. H. Kwak, J. Wang, V. V. Viswanathan, C. Wang, Y. Lin, Y. Wang, I. A. Aksay, J. Liu, *Electrochem. Commun.* **2009**, *11*, 954–957.
[14] J. Ma, J. N. Wang, *Chem. Mater.* **2008**, *20*, 2895–2902.
[15] a) Z. P. Wu, B. Y. Xia, J. N. Wang, *J. Power Sources* **2010**, *195*, 21432148; b) X. X. Wang, J. N. Wang, L. F. Su, *J. Power Sources* **2009**, *186*, 194–200.
[16] a) J. N. Wang, L. Zhang, J. J. Niu, F. Yu, Z. M. Sheng, Y. Z. Zhao, H. Chang, C. Pak, *Chem. Mater.* **2007**, *19*, 453–459; b) Z. M. Sheng, J. N. Wang, *Adv. Mater.* **2008**, *20*, 1071–1075; c) B. Y. Xia, J. N. Wang, X. X. Wang, J. J. Niu, Z. M. Sheng, M. R. Hu, Q. C. Yu, *Adv. Funt. Mat.* **2008**, *18*, 1790–1798; d) B. Y. Xia, J. N. Wang, X. X. Wang, *J. Phys. Chem. C* **2009**, *113*, 18115–18120.
[17] a) W. Bi, T. F. Fuller, *J. Electrochem. Soc.* **2008**, *155*, B215–221; b) D. A. Stevens, J. R. Dahn, *Carbon* **2005**, *43*, 179–188; c) O. A. Baturina, S. R. Aubuchon, K. J. Wynne, *Chem. Mater.* **2006**, *18*, 1498–1504; d) O. A. Pinchuk, S. R. Aubuchon, C. Marks, R. Dominey, F. Dundar, O. F. Deniz, A. Ata, K. J. Wynne1, *Fuel Cells* **2009**, *9*, 554–561.
[18] B. D. McNicol, *J. Electroanal. Chem.* **1981**, *118*, 71–87.
[19] a) S. J. Lee, S. Mukerjee, J. McBreen, Y. W. Rho, Y. T. Kho, T. H. Lee, *Electrochim. Acta* **1998**, *43*, 3693–3701; b) J. Perez, E. R. Gonzalez, E. A. Ticianelli, *Electrochim. Acta* **1998**, *43*, 1329–1339; c) E. Antolini, L. Giorgi, A. Pozio, E. Passalacqua, *J. Power Sources* **1999**, *77*, 136–142; d) E. P. Lee, Z. Peng, D. M. Cate, H. Yang, C. T. Campbell, Y. Xia, *J. Am. Chem. Soc.* **2007**, *129*, 10634–10635.
[20] a) P. J. Ferreira, G. J. laO, Y. S. Horn, D. Morgan, R. Makharia, S. Kocha, H. A. Gasteiger, *J. Electrochem. Soc.* **2005**, *152*, A2256–2271; b) Y. Shao-Horn, W. C. Sheng, S. Chen, P. J. Ferreira, E. F. Holby, D. Morgan, *Top. Catal.* **2007**, *46*, 285–305; c) W. Bi, T. F. Fuller, *J. Power Sources* **2008**, *178*, 188–196.
[21] a) T. C. Kuo, R. L. McCreery, *Anal. Chem.* **1999**, *71*, 15531560; b) J. L. Figueiredo, M. F. R. Pereira, M. M. A. Freitas, J. J. M. Orfao, *Carbon* **1999**, *37*, 1379–1389.
[22] a) X. Yu, S. Ye, *J. Power Sources* **2007**, *172*, 133–144; X. Yu, S. Ye, *J. Power Sources* **2007**, *172*, 145–154; b) M. Kang, Y. S. Bae, C. H. Lee, *Carbon* **2005**, *43*, 1512–1516.
[23] a) Y. Li, F. P. Hu, X. Wang, P. K. Shen, *Electrochem. Commun.* **2008**, *10*, 1101–1104; b) S. Wang, S. P. Jiang, T. J. White, J. Guo, X. Wang, *Adv. Funct. Mater.* **2010**, DOI: 10.1002/adfm.200900772.
[24] A. Guerrero-Ruiz, P. Badenes, I. R. Ramos, *Appl. Catal. A* **1998**, *173*, 313–321.
[25] a) Y. Tang, L. Zhang, Y, Wang, Y. Zhou, Y. Gao, C. Liu, W. Xing, T, Lu, *J. Power Sources* **2006**, *162*, 124–131; b) A. Stoyanova, V. Naidenov, K. Petrov, I. Nikolov, T. Vitanov, E. Budevski, *J. Appl. Electrochem.* **1999**, *29*, 1197–1203; c) A. Kabbabi, R. Faure, R. Durand, B. Beden, F. Hahn, J. M. Leger, C. Lamy, *J. Electroanal. Chem.* **1998**, *444*, 41–53.

[26] a) A. Kongkanand, S. Kuwabata, G. Girishkumar, P. Kamat, *Langmuir*, **2006**, *22*, 2392–2396; b) Z. Chen, M. Waje, W. Li, Y. Yan, *Angew. Chem.* **2007**, *119*, 4138–4141; *Angew. Chem. Int. Ed.* **2007**, *46*, 4060–4063; c) S. Zhang, X. Yuan, H. Wang, W. Merida, H. Zhu, J. Shen, S. Wu, J. Zhang, *Int. J. Hydrogen Energy* **2009**, *34*, 388–404.
[27] K. J. J. Mayrhofer, J. C. Meier, S. J. Ashton, G. K. H. Wiberg, F. Kraus, M. Hanzlik, M, Arenz, *Electrochem. Commun.* **2008**, *10*, 1144–1147.
[28] L. M. Roen, C. H. Paik, T. D. Jarvic, *Electrochem. Solid-State Lett.* **2004**, *7*, A19–22.
[29] a) K. J. J. Mayrhofera, S. J. Ashtona, J. C. Meiera, G. K. H. Wiberga, M. Hanzlikb, Ma. Arenza, *J. Power Sources* **2008**, *185*, 734–739; b) A. Stassi, E. Modica, V. Antonucci, A. S. Aricò, *Fuel Cells* **2009**, *9*, 201–208; c) S. Maass, F. Finsterwalder , G. Frank, R. Hartmann, C. Merten, *J. Power Sources* **2008**, *176*, 444–451; d) Y. Shao, G. Yin, J. Zhang, Y. Gao, *Electrochim. Acta* **2006**, *51*, 5853–5857; e) L. Li, Y. Xing, *J. Power Sources* **2008**, *178*, 75–79.

Received: March 26, 2010
Published online: June 16, 2010

